Biochimica et Biophysica Acta 1838 (2014) 2919–2928

Contents lists available at ScienceDirect

Biochimica et Biophysica Acta

journal homepage: www.elsevier.com/locate/bbamem

Global fold and backbone dynamics of the hepatitis C virus E2 glycoprotein transmembrane domain determined by NMR

Hila Shalom-Elazari [1], Hadas Zazrin-Greenspon [1], Hadassa Shaked, Jordan H. Chill *

Department of Chemistry, Bar Ilan University, Ramat Gan 52900, Israel

ARTICLE INFO

Article history:
Received 20 January 2014
Received in revised form 30 June 2014
Accepted 22 July 2014
Available online 7 August 2014

Keywords:
Hepatitis C virus
Envelope glycoproteins
Nuclear magnetic resonance
Protein structure
Membrane-associated proteins
Transmembrane helix

ABSTRACT

E1 and E2 are two hepatitis C viral envelope glycoproteins that assemble into a heterodimer that is essential for membrane fusion and penetration into the target cell. Both extracellular and transmembrane (TM) glycoprotein domains contribute to this interaction, but study of TM–TM interactions has been limited because synthesis and structural characterization of these highly hydrophobic segments present significant challenges. In this NMR study, by successful expression and purification of the E2 transmembrane domain as a fusion construct we have determined the global fold and characterized backbone motions for this peptide incorporated in phospholipid micelles. Backbone resonance frequencies, relaxation rates and solvent exposure measurements concur in showing this domain to adopt a helical conformation, with two helical segments spanning residues 717–726 and 732–746 connected by an unstructured linker containing the charged residues D728 and R730 involved in E1 binding. Although this linker exhibits increased local motions on the ps timescale, the dominating contribution to its relaxation is the global tumbling motion with an estimated correlation time of 12.3 ns. The positioning of the helix–linker–helix architecture within the mixed micelle was established by paramagnetic NMR spectroscopy and phospholipid-peptide cross relaxation measurements. These indicate that while the helices traverse the hydrophobic interior of the micelle, the linker lies closer to the micelle perimeter to accommodate its charged residues. These results lay the groundwork for structure determination of the E1/E2 complex and a molecular understanding of glycoprotein heterodimerization.

1. Introduction

Hepatitis C is the second most common chronic viral disease worldwide, with an estimated 180 million people afflicted by the disease or identified as carriers. It is caused by the hepatitis C virus (HCV) of the flaviviridiae family, and symptoms include chronic hepatitis, cirrhosis, hepatic carcinomas and extra-hepatic diseases [1,2]. It presents a major concern in healthcare systems as it can be transmitted via blood transfusion, organ transplantation and improperly sterilized surgical equipment. Understanding of HCV biology is surprisingly limited when considering its prevalence and significance in human health. As a result, existing therapeutic measures are often less than satisfactory, characterized by mediocre response levels and undesirable side-effects [3–5], although novel promising therapeutic strategies have been introduced lately [6–8]. The HCV genome encodes a polypeptide precursor which is ~3000 amino acids long and undergoes post-translational modification and cleavage into over 10 mature proteins [3,9,10]. Of these, the structured proteins, the core protein and envelope glycoproteins E1 and E2, form the viral particle, while the non-structured proteins are involved in the replication cycle and its regulation through protease, helicase and polymerase activities [11].

The envelope glycoproteins E1 and E2 are type I membrane-embedded proteins (MPs), each comprised of a large N-terminal ectodomain, a single membrane spanning domain and a short C-terminal cytoplasmic tail. They assemble into a heterodimer which allows the virus to fuse to the host membrane and thus is a critical contributor to its ability to insert its genetic material [12]. The structure of an E2-core/antibody complex was recently determined, showing the E2 ectodomain to form an immunoglobulin-fold β-sandwich flanked by additional protein layers [13]. Well established is the interaction between the two ectodomains and cell-surface receptors, accounting for their contribution to the fusion process [14–17]. In particular, the E2 ectodomain recognizes the host tetraspannin CD81 receptor, leading to membrane fusion and viral entry [15,18,19]. In addition, current studies have focused on anti-E2 antibodies [20] or E2-derived peptides [21] as potential HCV therapies. The importance of the stem region,

Abbreviations: 4-HTB, 4-hydroxy-2,2,6,6-tetramethylpiperidine 1-oxyl benzoate; CPMG, Carr–Purcell–Meiboom–Gill; DSS, 4,4-dimethyl-4-silapentane-1-sulfonic acid; HCV, hepatitis C virus; hetNOE, hetero-nuclear $\{^1H\}$-^{15}N-nuclear Overhauser effect; HSQC, heteronuclear single-quantum coherence; LPPG, 1-palmitoyl-2-hydroxy-sn-glycero-3-phospho-(1′-rac-glycerol); MBP, maltose-binding protein; MP, membrane-embedded protein; NOE, nuclear Overhauser effect; PRE, paramagnetic relaxation enhancement; SD, standard deviation; SL, spin-label; TEV, tobacco etch virus; TM, transmembrane; TROSY, traansverse-relaxation optimized spectroscopy

* Corresponding author.
E-mail address: Jordan.Chill@biu.ac.il (J.H. Chill).

[1] These two authors contributed equally to the manuscript.

http://dx.doi.org/10.1016/j.bbamem.2014.07.023
0005-2736/

preceding the hydrophobic membrane-inserted region, has been similarly demonstrated [22–24]. In contrast, the contributions of the glycoprotein transmembrane (TM) domains are poorly understood due to the challenging nature of structural studies in MPs. Besides directing and anchoring E1 and E2 to the endoplasmic reticulum and acting as signal sequences, the E1 and E2 TM domains contribute to the affinity of the glycoprotein heterodimer. Mostly hydrophobic in nature, the TM domains do uncharacteristically contain charged residues as well, K^{370} on E1 and both D^{728} and R^{730} on E2 [25–27]. Notably, mutations at these positions and at the G^{354}VLAG^{358} element of E1 result in a 3- to 4-fold reduction in heterodimer formation and cellular fusion assays [26,27] (Fig. 1A). While the TM-domains are predicted to be α-helical, structural information in a biological environment is currently unavailable.

The heterodimer of E1 and E2 TM domains forms a bitopic system, an assembly common to over half of membrane-associated proteins (MPs) in analyzed genomes [28]. Pathology-causing mutations have been found in several bitopic systems, highlighting the role played by these domains in both health and disease [29,30]. In bitopic systems two single-TM helical MPs assume a parallel orientation and associate within the membrane via non-covalent interactions. The reversible association between two membrane-spanning domains is a well-known paradigm for cellular signaling [31], and has attracted significant attention in recent studies [32]. Structural studies of MPs are hampered by the need for solubilizing the protein in a membrane-mimicking environment, making it harder to obtain homogeneous samples and increasing the effective size of the structural target. For purposes of study by high-resolution NMR MPs are typically stabilized in micelles or disk-like bicelles formed by detergents or phospholipids [33–36] or assembled nano-discs [37,38], while solid-state NMR studies utilize phospholipid bicelles, vesicles or oriented bilayers for stabilization of membrane peptides [39–42]. Generally, NMR offers the dual advantage of structural investigation under close-to-native conditions, and sensitivity to dynamic processes on a wide range of timescales unobservable using other methods [43–45]. In addition, several NMR-based methods are available for studying protein-protein interactions even with low affinities [45–48]. The latest achievements of NMR in addressing MPs and specifically bitopic systems have been presented in excellent recent reviews [32,49].

In light of the importance of a structural understanding of E1/E2 heterodimerization, and pursuant to our previous investigation of the E1 membrane-spanning domain [50], we have applied solution NMR to characterize the TM domain of E2 (E2-TM) from the HCV envelope glycoprotein. We have successfully produced and purified a double Cys-to-Ser mutant version of this peptide as a maltose-binding protein (MBP) fusion polypeptide, and characterized its behavior in 1-palmitoyl-2-hydroxy-sn-glycero-3-phospho-(1′-rac-glycerol) (LPPG) micelles. The micelle-spanning region was defined as residues 717–746, and was shown to contain two helical regions connected by a non-helical hinge linker that coincides with charged residues D728 and R730. Analysis of relaxation rates indicates increased flexibility in the linker region, although the dominating motion remains the global tumbling of the mixed micelle, with an estimated correlation time of 12.3 ns. Paramagnetic spectroscopy and cross-relaxation measurements suggest that the helical segments span the hydrophobic micelle interior, while the linker is located closer to the micelle perimeter, thereby accommodating the unpaired charged residues in E2-TM. Thus, binding of E1-TM to E2-TM may significantly affect its structure and orientation within the biological membrane.

2. Experimental

2.1. Media and solvents

DNA primers, the Isogro-DCN supplement for triply labeled media and 4-hydroxy-2,2,6,6-tetramethylpiperidine 1-oxyl benzoate (4-HTB) were obtained from Sigma-Aldrich (St. Louis, MO, USA). Isotopically labeled chemicals for constructing labeling media, including $^{2}H_2O$, ^{13}C-labeled glucose and $^{15}NH_4Cl$, were purchased from Cambridge Isotope Laboratories (Andover, MA, USA). LPPG was purchased from Avanti Polar Lipids, Inc. (Alabaster, AL, USA). M9 minimal media was made as previously described [51], with substitution of $^{15}NH_4Cl$, $^{13}C_6$-glucose and $^{2}H_2O$ for producing triply-labeled E2-TM. HPLC grade solvents HCOOH and isopropanol were purchased from Biolabs (Jerusalem, Israel).

2.2. Cloning of the E2-TM sequence

Cloning of the double mutant construct MBP-$(His)_6$-TEV-E2-Arg_6 C732S/C734S was performed in three steps. First the coding sequence of E2-TM (purchased from GeneArt, Germany) was inserted into a pETMBPH vector, a modified pET28a(+) construct containing the maltose binding protein (MBP) coding sequence [52], using a restriction site-free cloning method between the *Kpn*I restriction site and stop codon [53]. Next, the Arg_6 segment was inserted following E2-TM sequence (*vide infra*) to increase solubility. Each of the primers ((phos)-Arg6-5′ and Arg6-3′) was designed with an additional coding sequence for three arginine residues, and PCR reaction followed by ligation yielded the desired vector (also confirmed by DNA sequencing). In the last PCR reaction site directed mutagenesis using primers (phos)-CysToSer-5′ and CysToSer-3′ followed by ligation provided the final MBP-His-Tev-E2-Arg6 C732S/C734S construct. The final plasmid was amplified in *Escherichia coli* DH5α cells and its sequence confirmed, and it was used to transform an *E. coli* BL21(DE3) expression system.

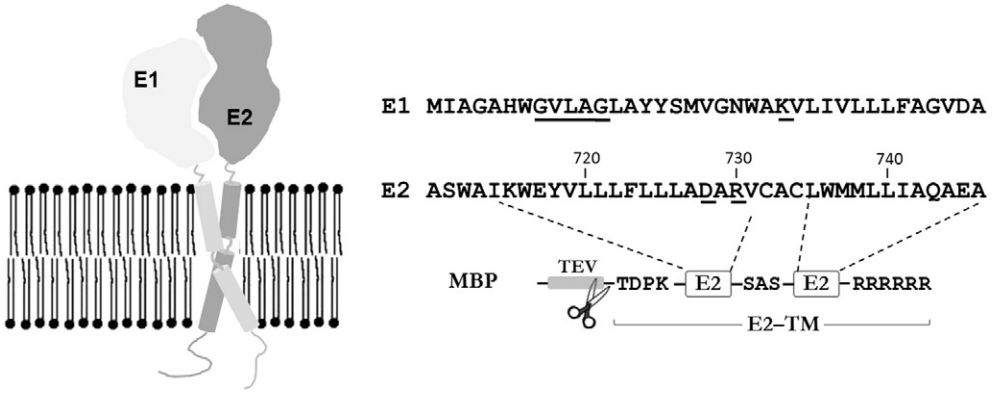

Fig. 1. The E1/E2 glycoprotein heterodimeric system in HCV. Left, schematic representation of the HCV E1 (light gray) and E2 (dark gray) glycoproteins, emphasizing the segments embedded in the viral membrane. Right, membrane-spanning sequences of E1 and E2 with residues known to be involved in heterodimerization underlined. Below, the E2-TM construct in detail.

2.3. Expression and purification of the E2-TM peptide

E2-TM expression was performed in M9 minimal medium [51], and ^{15}N- and ^{13}C-isotope labeling were achieved using 1 g/L 99% $^{15}NH_4Cl$ and 2.5 g/L 99% $^{13}C_6$-glucose, respectively. The expression protocol closely followed the procedure used to express a similar membrane-spanning peptide in an earlier study [50]. Briefly, IPTG-induced cultures were grown overnight at 27 °C and harvested by centrifugation. For purification of E2-TM cells were lysed by homogenization (C5 homogenizer, Avestin) and the MBP-tethered E2-TM was captured by Ni^{2+}-affinity chromatography. This fraction was collected, dialyzed overnight and incubated with TEV protease (1:10 wt\wt) for 3–5 h at 30 °C, resulting in quantitative cleavage (>95%) of the E2-TM peptide from its MBP carrier. The peptide was then separated from MBP by preparative reverse-phase HPLC on a C4 column (Phenomenex, Torrance, CA, USA) using a H_2O/isopropanol linear gradient (30:70 to 50:50) containing 10% (vol/vol) formic acid at 60 °C (Supporting Information, Figure S1). E2-TM-containing fractions were pooled and lyophilized in preparation for solubilization in phospholipid for NMR experiments. Protein concentration was determined by measuring the absorbance at 280 nm, based on a specific absorbance of 2.3 OD_{280} for a 1 mg/ml solution.

2.4. Circular dichroism measurements

CD experiments were acquired on a Chirascan polarimeter (Applied Photophysics) for a 15 μM sample of LPPG-solubilized E2-TM in 20 mM NaPi buffer, pH 6.5, placed in a temperature-controlled cuvette with a 0.1 cm pathlength. The experiment was repeated three times and subtracted from a measurement of an identical buffer sample. Results were analyzed using the MP180 module of the DichroWeb platform for the 190–240 nm range [54].

2.5. NMR spectroscopy

All 2D- and 3D-NMR measurements were conducted on a DRX700 Bruker spectrometer using a cryogenic triple-resonance TCI probehead equipped with z-axis pulsed field gradients. Sample conditions for all E2-TM preparations were 0.2–0.5 mM peptide in buffer containing 20 mM phosphate buffer, with pH values of 6.0–6.5, 20 mM NaCl, 7% ^2H_2O, and 40 mM of the phospholipid LPPG. Samples were placed in Shigemi (Shigemi, Allison, PA, USA) or Wilmad (Wilmad Labglass, Vineland, NJ, USA) NMR tubes. Measurements were conducted (unless stated otherwise) at 318 K. TROSY- (*tr*-) and non-TROSY versions of the ^1H,^{15}N-HSQC for screening of measurement conditions were acquired using a standard sequence run for 30–60 minutes. For backbone assignment, TROSY-based triple resonance HNCO, HNCA, HN(CO)CACB, and HNCACB experiments using sensitivity-enhanced echo-antiecho detection [55] were acquired for triply labeled ^2H,^{13}C,^{15}N-E2-TM. Triple-resonance experiments were typically acquired with 512 complex points and an acquisition time of 52.2 ms in the observed dimension and 32–36 complex points and an acquisition time of 20.2–22.8 ms in the ^{15}N dimension. In the ^{13}C dimension, experiments with ^{13}CO ($^{13}C^{\alpha}$) evolution were acquired with 32–40 complex points and 21.2–26.5 (7–7.5) ms acquisition time, and experiments with $^{13}C^{\alpha/\beta}$ evolution were acquired with 56–64 complex points and 5.3–6.1 ms acquisition time. All spectra were processed using the TopSpin 2.1 package (Bruker BioSpin, Karlsruhe, Germany). Chemical shifts were referenced indirectly against 4,4-dimethyl-4-silapentane-1-sulfonic acid (DSS).

Relaxation measurements were conducted in scan-by-scan interleaved fashion with a *tr*-HSQC spectrum for readout at static magnetic field of 16.4 T and 318 K. Longitudinal relaxation rates (R_1) were estimated from a series of decay spectra with delays of 2 (reference spectrum), 252, 502, 752, 1002, and 1252 ms. Similarly, transverse relaxation rates (R_2) were estimated from a series of decay spectra acquired in CPMG-form with relaxation times of 16.96 (reference spectrum), 33.92, 50.88, 67.84, 84.80, and 101.76 ms. The heteronuclear ^{15}N-{^1H}-NOEs (hetNOEs) were determined by recording pairs of interleaved spectra with and without proton saturation during the recycle delay, with similar acquisition times in both dimensions. In each measurement a total of 32–40 transients were collected per t_1 experiment and delays between scans were 3.0 s; in the hetNOE experiment this delay was set to 5.9 s. Total experiment time for each relaxation measurement was 60–72 h. For extraction of R_1 and R_2 relaxation intensities were fit to an exponential decay function using the Bruker TopSpin 2.1 Dynamics suite, and hetNOEs were derived from the intensity ratio in reference and attenuated spectra. Analysis of relaxation rates using the model-free approach was performed using the Matlab-based DYNAMICS program [56,57].

The rate of exchange of amide protons with bulk ^2H_2O-based solution was estimated by comparing two *tr*-HSQC spectra, one acquired for a 0.2 mM sample of ^2H,^{13}C,^{15}N-labeled E2-TM, and the other after 7-fold dilution with ^2H_2O-based buffer of otherwise identical composition. In spin-label- (SL)-mediated relaxation measurements the intensity ratio of *tr*-HSQC cross-peaks before and after addition of the stable nitroxide radical 4-hydroxy-2,2,6,6-tetramethylpiperidine 1-oxyl benzoate (4-HTB) (final concentration 0.2 mg/ml) was used as a measure of the proximity of each amide proton to the unpaired electron. For cross-relaxation effects between micelle protons and the E2-TM amide protons a *tr*-HSQC experiment was preceded by a l.2 s irradiation period followed by a 0.6 s recovery delay. Irradiation was centered at 2.8 kHz upfield of the LPPG ^1H signals as a control and in turn upon the LPPG methyl group, overlapping methylene groups (H^{4-15}) and the penultimate methylene (H^3), all in interleaved fashion. Selective irradiation (as verified by observing its effects on the LPPG ^1H-NMR spectrum) was achieved using repeated REBURP inversion pulses with a maximum γB_1 of 208.8 Hz.

3. Results

3.1. Biosynthesis of E2-TM and sample preparation

Due to their hydrophobicity, TM domains are notoriously difficult to prepare using solid-phase synthesis methods, since they exhibit a strong aggregation tendency that limits the efficiency of amino acid coupling. We therefore employed recombinant techniques to express the E2 transmembrane domain peptide fused to a carrier protein designed to enhance expression levels and solubility following a strategy that proved successful in a previous study of the E1 membrane spanning domain. This avoided aggregation of the hydrophobic E2 membrane-spanning peptide during expression and purification, and still allowed later separation between carrier protein and peptide after cleavage using reverse-phase HPLC methods [50]. The E2 peptide was chosen from a consensus sequence of viral strains and based on a previous prediction of the membrane spanning region as including residues 714–746 [58,59]. In the course of optimizing expression and purification protocols we established two additional factors influencing the final yield of the purified E2-derived peptide, (i) addition of charged residues to the hydrophobic peptide to increase its solubility once the carrier protein is removed, and (ii) mutation of two cysteine residues in the E2 sequence to avoid intermolecular disulfide bridging and consequent oligomerization. Previous studies had not established an involvement in binding for these cysteine residues [26,27]. Accordingly, the final construct fashioned, affording peptide yields sufficient for the NMR study, included maltose binding protein (MBP) linked by a tobacco etch virus (TEV) protease cleavage site to the double Cys-to-Ser mutant E2 peptide followed by a hexa-arginine tail. An additional five residues preceded this sequence due to cloning considerations. Overall, the final 44-mer double-mutant peptide used in this study was (GTDPK) I^{714}KWEYVLLLFLLLADARVSASLWMMLLIAQAEA^{746}(RRRRRR), referred to as E2-TM (Fig. 1B). Expression and purification of this construct

closely followed the aforementioned strategy [50], yielding a lyophilized E2-TM peptide which could be solubilized in a detergent of choice in preparation for NMR and CD experiments.

3.2. Structural characterization of E2-TM in LPPG micelles

Previous studies have established that the choice of detergent for solubilization of membrane peptides is a critical factor in obtaining NMR-amenable samples with biological relevance [33–36]. We used 1-palmitoyl-2-hydroxy-sn-glycero-3-phospho-(1′-rac-glycerol) (LPPG), a phospholipid known to be generally suitable for NMR studies of membrane proteins [33] to solubilize lyophilized E2-TM. Circular dichroism (CD) characterization of E2-TM in LPPG micelles produced a curve with characteristic minima at 208 and 222 nm, indicating the prevalence of α-helical secondary structure (Fig. 2A). Using the DichroWeb MP180 module for analyzing CD results of membrane-embedded peptides [54] we determined the proportion of helical character in E2-TM to be 40%. This value is consistent with our expectation that E2-TM adopts a helical conformation in the membrane-mimicking environment.

A comparison between the relaxation-optimized (TROSY) and regular versions of the $^{1}H,^{15}N$-HSQC indicated that the former afforded better signal-to-noise for E2-TM (Supporting Information, Figure S2) and was subsequently utilized for evaluating the quality of NMR samples. The TROSY-HSQC (*tr*-HSQC) NMR spectrum of this sample provided further evidence that E2-TM was stabilized in native conformation by LPPG micelles. A 0.25 mM E2-TM sample at a temperature of 318 K and a static magnetic field of 16.4 T afforded a well-resolved spectrum within 20-30 minutes of measurement time. Although some overlap between cross-peaks was observed, as is characteristic of helical proteins, 33 resolved backbone $^{1}H–^{15}N$ moieties (of the expected 36) could be detected in the spectrum. Two indole $^{1}H–^{15}N$ groups, emanating from residues W716 and W736, were clearly seen, and the ^{15}N upfield region of the spectrum was devoid of peaks, as expected for E2-TM which lacks glycine residues (Fig. 2B). Membrane peptides poorly stabilized and suffering from hydrophobic mismatch or aggregation typically exhibit a weak *tr*-HSQC spectrum due to heterogeneous dispersion in the membrane-mimicking environment or exchange-mediated spectral broadening [33,34,36,60]. Therefore, experimental evidence is consistent with a well-behaved sample of sufficiently pure E2-TM amenable to further study by NMR.

A ^{2}H, ^{13}C, ^{15}N-triply labeled E2-TM peptide was used to acquire TROSY versions of the HNCO, HNCA, HN(CO)CACB, and HNCACB experiments [55] at 318 K. The HNCO experiment correlated each $^{1}H,^{15}N$-pair with the $^{13}C'$ nucleus of the preceding residue, alleviating any overlap between HSQC peaks and affording chemical shifts of carbonyl nuclei. The other three experiments similarly correlated each $^{1}H,^{15}N$-pair with the two adjacent $^{13}C^{\alpha}$ nuclei (in the case of the HNCA), the $^{13}C^{\alpha}/^{13}C^{\beta}$ of the preceding residue (in the case of the HN(CO)CACB) and the two adjacent $^{13}C^{\alpha}/^{13}C^{\beta}$ pairs (in the case of the HNCACB). The combination of these spectra was sufficient to assign peptide backbone and $^{13}C^{\beta}$ chemical shifts utilizing well known methodologies [61]. Fig. 2C shows typical strip-plots demonstrating the 'backbone-walk' based on these connectivities and the resulting assignment of the fingerprint *tr*-HSQC spectrum (Fig. 2B). The resonance assignment of E2-TM solubilized in LPPG micelles has been deposited in the Biological Magnetic Resonance Data Bank (BMRB), under accession code 19636.

3.3. Secondary structure in LPPG-solubilized E2-TM

Secondary chemical shifts are an excellent indicator of secondary structure in proteins [62–65]. Analysis of $^{13}C'$, $^{13}C^{\alpha}$, and $^{13}C^{\beta}$ secondary chemical shifts for LPPG-solubilized E2-TM shows the peptide to adopt a helical conformation. Secondary chemical shifts exhibited typical values

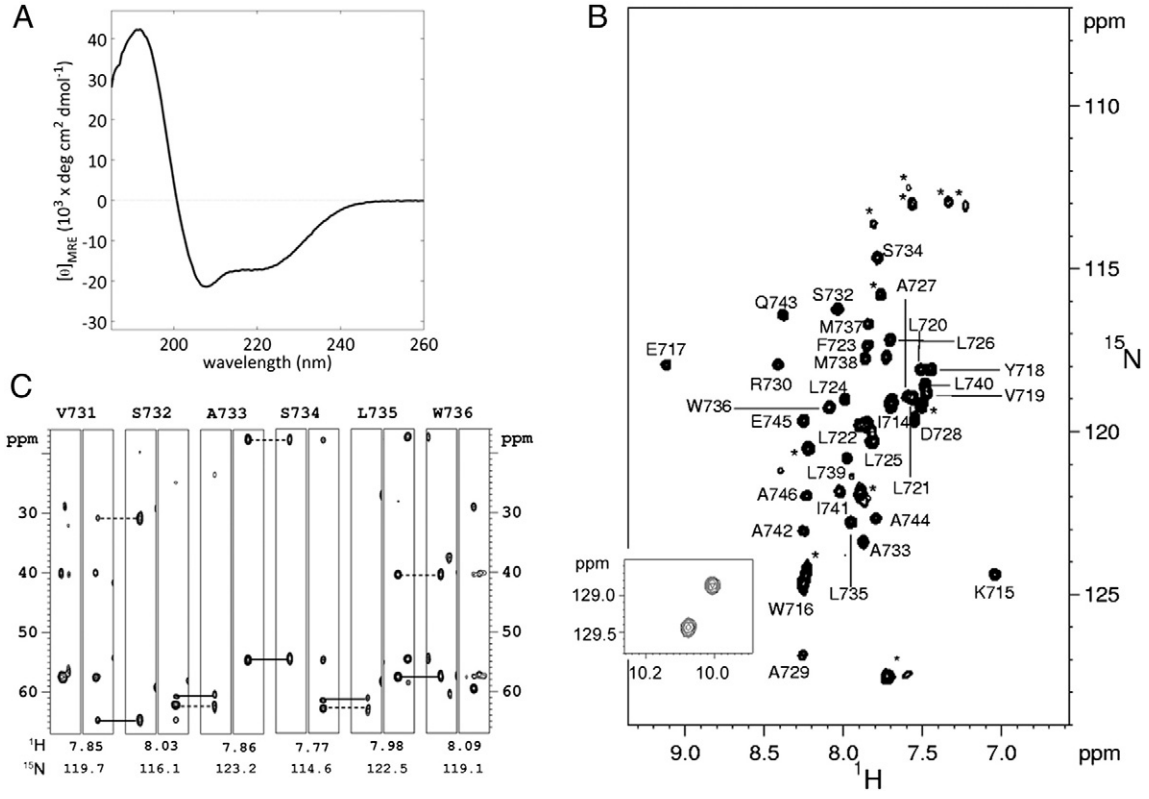

Fig. 2. Characterization of E2-TM solubilized in LPPG micelles. (A) CD curve for E2-TM in 20 mM NaPi pH 6.8, 10 mM NaCl, 40 mM LPPG at 318 K. (B) *tr*-$^{1}H,^{15}N$-HSQC spectrum of E2-TM with annotation of amide peaks. The inset shows the indole ring cross-peaks of W716 and W736. Asterisks denote cross-peaks from sidechain or non-E2 residues $^{1}H-^{15}N$ pairs. (C) Strips from the *tr*-HN(CO)CACB (left in every pair) and *tr*-HNCACB (right in every pair) spectra of E2-TM in LPPG micelles, demonstrating the 'backbone walk' between adjacent residues allowing assignment of resonances. Here this is shown for residues $V^{731}SASLW^{736}$, with $^{13}C\alpha$ ($^{13}C\beta$) resonances connected in solid (dashed) lines.

of helical conformation, +2 to +3 for $^{13}C'$ and $^{13}C\alpha$ nuclei and −1.5 to −2 for $^{13}C\beta$ nuclei in two segments spanning residues 717–726 (α1) and 732–746 (α2). For residues 714–715 and 727–730 and the non-native E2-TM residues secondary chemical shifts were far less significant, indicating the boundaries of the E2-TM helical regions (Fig. 3). In particular, residues connecting the two helices appear to be an unstructured linker that coincides with the location of charged residues D728 and R730. Analysis of secondary chemical shift data using the TALOS platform [66] exhibited an average helical population of 80% for α1 residues and 90% for α2 residues, as opposed to 40% for the linker residues 727–730, whose random coil population exceeded 50% (Fig. 3, bottom panel).

Confirmation of these findings was obtained from a measurement of amide proton exchange rates upon exposure to ^2H_2O. Typically these rates are estimated by following signal loss upon transfer of the sample to ^2H_2O. However, solubilization of lyophilized E2-TM in the presence of phospholipid is relatively time-consuming, dictating a more qualitative and useful measure of exchange rates. A ^2H,^{13}C,^{15}N-labeled E2-TM sample was diluted 7-fold into an identical ^2H_2O-based buffer, and *tr*-HSQC spectra before and after dilution were compared, with the length of the second experiment adjusted to match the signal-to-noise level of the initial one. Since both exchange and relaxation rates contribute to the results, a quantitative interpretation of the intensity ratio between the two experiments is not straightforward. However, on the qualitative level exchangeable amide protons quickly reflect the new H_2O:^2H_2O ratio, whereas protected sites show an excess of protonated amides. E2-TM amide protons exhibiting relative protection from solvent exchange included residues 720–726 and 738–743. Both segments are found within the two known helices, including central helix residues but not those in the first 1–2 helical turns (Fig. 4). The main contribution to protection from exchange is provided by a combination of hydrogen-bonding accompanying secondary structure and accessibility to bulk solvent, closely correlated to the radial positioning within the micelle. Overall, results of both chemical shift and solvent exposure experiments confirm the location of the two helices in E2-TM and are consistent with a helix–linker–helix arrangement.

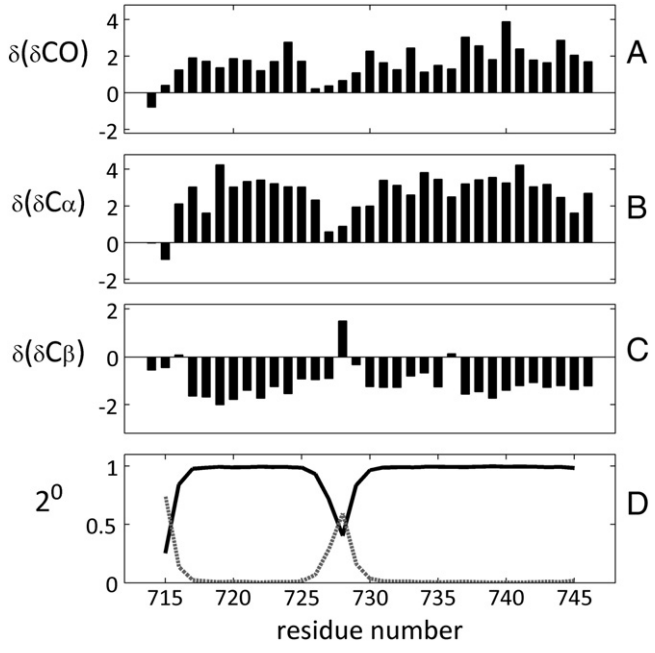

Fig. 3. Secondary chemical shifts of E2-TM define its helical nature. Secondary chemical shifts measured along the E2-TM backbone. Shown are values for (A) $^{13}C'$, (B) $^{13}C^{\alpha}$, (C) $^{13}C^{\beta}$ nuclei in LPPG micelles. (D) TALOS [66] predicted populations in helical (solid black line) and random coil (gray line) conformations.

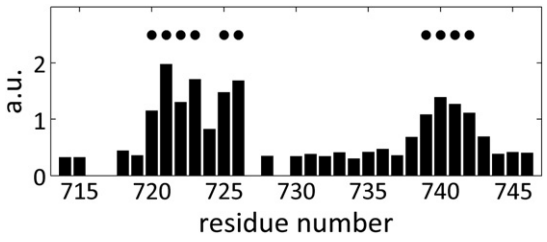

Fig. 4. Amide proton exchange rates of the E2-TM peptide in LPPG micelles. Bars show the ratio between *tr*-HSQC peaks acquired for a 0.4 mM sample of E2-TM in LPPG micelles in 7% ^2H_2O (80 min) and the same sample immediately after 7:1 dilution into ^2H_2O-based buffer (12 h). Fast amide proton exchange and relaxation dictate a ~0.35 ratio for fully exchangeable protons. Residues with a 3-fold higher ratio or more are denoted with filled circles.

3.4. Order and flexibility on the ps–ns timescale along the E2-TM sequence

^{15}N relaxation rates are a well-accepted reporter on global and local motions on the ps–ns timescale in the peptidic backbone [43,44]. R_1 and R_2 rates and hetNOEs were measured for LPPG-solubilized E2-TM at 318 K and 16.4 T. Two E2-TM segments, spanning residues 717–726 and 732–746, exhibited relaxation parameters consistent with rigid domains, in close agreement with the α1 and α2 helical regions identified earlier. Typical relaxation rates observed for the α1 (α2) segment (ranges are ±1 SD in all cases) were R_1 values of 0.88–0.94 (0.80–0.88) s^{-1}, R_2 values of 16.7–19.3 (16.0–20.0) s^{-1} and hetNOE values of 0.70–0.80 (0.76–0.84) (Fig. 5A). R_1 and R_2 rates of residue W716 (adjacent to α1), residues A727, D728, R730 and V731 in the linker region connecting the two helices (residue A729 afforded a cross-peak that was too weak for this analysis), and the two arginine residues adjacent to the α2 segment were similar to those of the helical region, although their hetNOE was lower. In contrast, residues preceding α1 and the last four arginine residues exhibited elevated R_1 values (1.14–1.28 s^{-1}) and reduced R_2 and hetNOE values (5–10 s^{-1} and 0.27–0.53, respectively) suggesting increased motions on the ps–ns timescale and flexibility in these regions (Fig. 5A). Together these results define the micelle-spanning region (residues 717–746) of the peptide, with residue W716 and the first two arginines representing transitional regions, most likely located at the phospholipid-water interface.

A more quantitative view of order and flexibility of all E2-TM residues (inside and outside the LPPG micelle) was afforded by reduced spectral density [67–69] and model-free [70,71] analyses of relaxation rates. The former determines the relative contributions of motions on different timescales to the overall relaxational behavior, and the latter differentiates specifically between contributions of local motions on the backdrop of a global molecular tumbling. The membrane spanning region is clearly identified by typical J_0 values of ~5 ns and negligible contributions of J_N and $J_{0.87H}$ values, and high generalized square order parameters ($0.85 < S^2 < 0.95$) with limited local motions. Local motions are more prevalent in α1 compared to α2, indicating the latter is more rigid. A sharp decrease in J_0 and S^2, and an increase in $J_{0.87H}$ and in local motions for the E2-TM termini indicates that these residues are located outside the micelle. The linker connecting α1 and α2 exhibited a small yet significant increase in faster motions (J_N and $J_{0.87H}$), while maintaining S^2 values indicative of rigidity. This suggests that despite the increased backbone motions, consistent with the lack of secondary structure in this segment, the helix–linker–helix architecture remains relatively well-ordered. Model-free analysis indicated a global tumbling time of 12.3 ± 0.3 ns for the E2-TM-containing micelle at 318 K. Based on the Stokes–Einstein equation for rotational diffusion of a spherical body, and assuming a viscosity of 0.59 cp for an aqueous sample at 318 K, this corresponds to a hydrodynamic radius of ca. 28 Å for the mixed LPPG micelle, in agreement with results of a previous study [72].

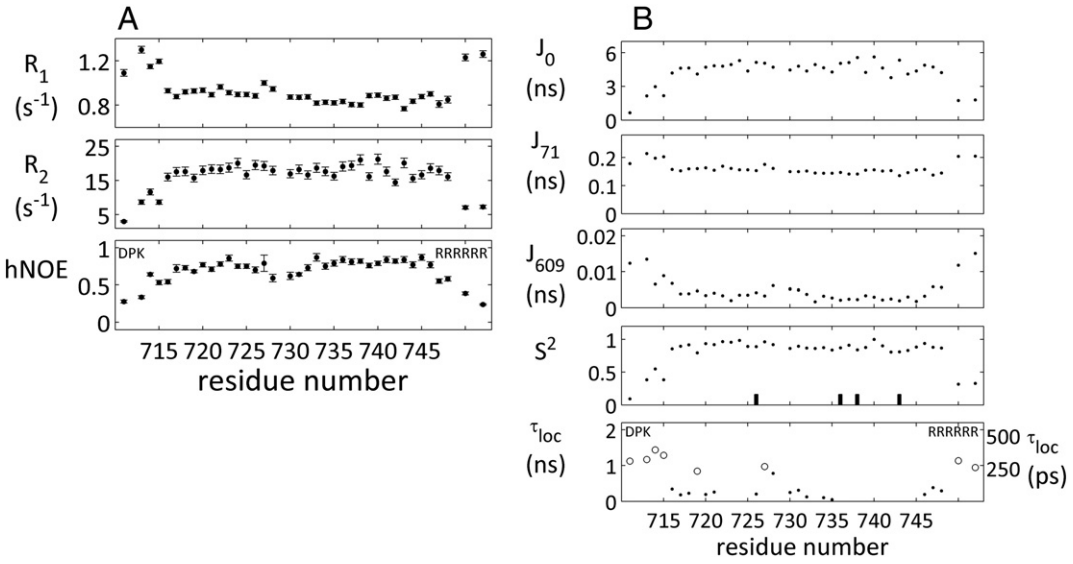

Fig. 5. Relaxation measurements report on ps–ns dynamics of the E2-TM-LPPG assembly. Backbone ^{15}N relaxation rates measured for $^{2}H,^{13}C,^{15}N$-labeled E2-TM at a static field of 16.4 T and 318 K. (A) Shown are longitudinal relaxation R_1 (top), transverse relaxation R_2 (middle) and the heteronuclear ^{15}N-{^{1}H}-NOE (bottom). Typical errors in relaxation rate measurements were 4-6%. (B) Analysis of relaxation rates using reduced spectral density mapping [67–69] (panels 1–3) and the model-free approach [70,71] (panels 4–5). Shown are the $J(0)$, $J(\omega_N)$ and $J(0.87\omega_H)$ contributions to relaxation at 16.4 T (panels 1–3). Also shown are the generalized squared order parameter (panel 4) and local backbone motions (panel 5) along the E2-TM sequence. In panel 4 dark bars designate residues for which the transverse relaxation rate suggested an exchange contribution. In panel 5 filled and empty circles represent motions on the ps (right axis) and the ns (left axis) timescales, respectively. In both figures, DPK and RRRRRR designate E2-TM residues which are not native to E2.

3.5. Structural characterization of mixed LPPG/E2-TM micelles

Our earlier findings established a helix–linker–helix architecture for E2-TM, and determined that the linker segment lacks secondary structure and exhibits marginal flexibility. To further characterize our system by determining the relative positioning of the peptide within the micelle, we added to the mixed micelle 0.2 mg/ml of 4-hydroxy-TEMPO benzoate (4-HTB), a water-insoluble nitroxide radical, and, after sonication to ensure its incorporation into the micelle, followed its paramagnetic effect upon the E2-TM peak intensities. Under these conditions a decrease in peak intensity should reflect a relaxation-enhancement effect due to the proximity of the unpaired electron to a given amide proton. Comparison of *tr*-HSQC spectra before and after addition of 4-HTB revealed a strong effect (decrease of 40%–50%) for residues 728-732, and a smaller yet still significant effect (20%–25%) for adjacent residues 733–735. In addition, the signals of several residues at the E2-TM termini were weakened in the presence of 4-HTB, in some cases (K715, K(−1) preceding the E2 residues, and R3,4,5 of the hexa-arginine tail) beyond detection (Fig. 6, top). Since the latter residues were previously located outside the micelle, this result is consistent with the linker being positioned near the micelle headgroups. It also predicates a more diffuse distribution of 4-HTB than anticipated.

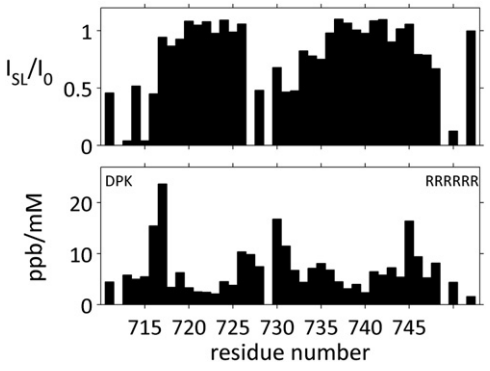

Fig. 6. Effect of paramagnetic spin-labels on E2-TM amide protons. Top, ratio of *tr*-HSQC peak after (I_{SL}) and before (I_0) the addition of 0.1 mg/ml 4-HTB to 0.2 mM E2-TM in 40 mM LPPG, 20 mM KPi buffer pH 6.7, 20 mM NaCl, and 0.01% NaN_3. Bottom, change in position of *tr*-HSQC peaks, defined as $\Delta_{HN} = (\Delta_H^2 + (\Delta_N/5)^2)^{½}$, where Δ_H and Δ_N are the individual change in ^{1}H and ^{15}N shifts, respectively, upon titration to final concentrations of 0–8 mM Mn^{2+}. Values shown are the change in Δ_{HN} in ppb per mM of titrated Mn^{2+}. DPK and RRRRRR designate E2-TM residues which are not native to E2.

With the aim of further confirming these results we followed changes in the E2-TM fingerprint spectrum during the course of a Mn^{2+} titration. The Mn^{2+} ion, unable to penetrate into the micelle, has an isotropic g-tensor, and is therefore expected to selectively enhance the relaxation of amide groups in its vicinity. Surprisingly, the E2-TM spectrum exhibited Mn^{2+}-induced chemical shift changes, indicating that the paramagnetic center had lost its symmetry. We attributed this to a binding of the ion to the mixed micelle, most likely to the phospholipid headgroup, largely in excess over other potential ligands such as negatively charged peptide residues. Fig. 6 (bottom) demonstrates the magnitude of this pseudocontact shift effect along the E2-TM backbone. While local effects may contribute to these effects, as reflected in the relatively large change in E717 and E745 chemical shifts, the general trend is of a more significant effect upon linker residues 727–731 than for the residues of the α1 and α2 helices. This further supports our earlier conclusion that the linker segment is removed from the micelle core and is located closer to the phospholipid headgroup.

We also employed a complementary approach for determining the location of E2-TM in the mixed micelle in order to avoid potential ambiguities arising from the distribution of the paramagnetic center within the micelle. Cross-correlated relaxation between phospholipid (or detergent) and peptide protons has been utilized in various ways to qualitatively estimate the position of the latter within the micelle [73–75]. Here we compared the effects of irradiation on protons of the palmitoyl chain upon the *tr*-HSQC of E2-TM. Generally, buildup of cross-relaxation was relatively slow, most likely due to shorter tumbling time of the mixed LPPG/E2-TM micelles when compared to other studied systems [73,75] and the fluidity of the LPPG micelle. Since intramolecular cross-relaxation between E2-TM protons is faster, this experiment identifies peptide segments in proximity with irradiated micelle protons rather than specific residues. As shown in Fig. 7, irradiation of the overlapping methylene protons (on carbons 4–15) provided the strongest effect on the E2-TM spectrum. Whereas a peptide oriented

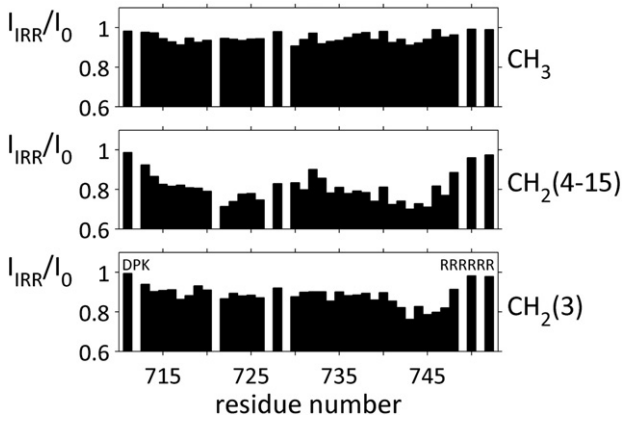

Fig. 7. Cross-relaxation between E2-TM and phospholipid protons. Cross-relaxation between various LPPG protons and the amide protons of E2-TM is estimated by measuring the ratio between *tr*-HSQC peaks with and without saturating irradiation on the LPPG protons. Experimental conditions are detailed in the text. Shown are the results for irradiation of the terminal methyl protons (top), the overlapping methylene groups on carbons 4–15 (middle) and the methylene protons on carbon 3 (bottom). Typical errors in I_{IRR}/I_0 values were 0.02–0.04. DPK and RRRRRR designate E2-TM residues which are not native to E2.

along the micelle diameter should exhibit a monotonous increase in magnetization transfer towards its center, E2-TM exhibits a clear trend of decreased transfer of magnetization in the linker region in comparison to the helical segments, and no apparent effect of irradiation of methyl protons upon linker signals. This confirms our previous conclusion that the linker region lies closer to the more polar headgroup region.

4. Discussion

Since heterodimerization of the E1/E2 glycoproteins is a mandatory step for fusion of viral and host cell membranes during infection by HCV [12,27], and interactions within their TM-domains contribute to this cellular event, inhibition of this interaction is a promising avenue for combating HCV infection. Currently there is very little structural information for E2-TM in a biologically relevant environment or for its complex with the E1-TM domain. These two considerations form the primary motivation for this study. A significant hurdle faced by structural investigations of membrane-embedded peptides is the need to synthesize them in sufficient amounts by chemical or recombinant methods, generally a challenging task due to their strong aggregation tendency during expression or purification [76]. We achieved this aim by fusing the E2-TM peptide via a linker containing a proteolysis cleavage site to the MBP C-terminus, adding a solubility-enhancing Arg_6 tag at the peptide C-terminus, and replacing the cysteine residues with serines to avoid covalent aggregation via disulfide bond formation. Together these factors allowed us to prepare E2-TM samples amenable to NMR study by solubilization in LPPG micelles, known to stabilize MPs sufficiently to allow acquisition of necessary NMR data [33]. Bicelles, assemblies formed by a mixture of short- and long-chain phospholipids have been proposed as an environment that ideally mimics the native bilayer and they are less prone to curvature effects [34,77].We note, however, that the estimated diameter of an LPPG micelle is in excess of ~50 Å, which should be sufficient to avoid hydrophobic mismatch effects in the E2-TM helices.

Well-established NMR methods were used to characterize the conformation adopted by E2-TM within the stabilizing micelles and the architecture of the E2-TM/LPPG macroassembly in terms of micellar size and positioning of the peptide. Findings of several experimental methods concur that E2-TM residues assume an α-helical conformation. Trp residue W716 demarcates the beginning of the membrane-embedded domain, located characteristically at the water-micelle interface. The first helical domain, α1, includes residues 717–726, and the second domain, α2, spans residues 732–746. Establishing the helical nature of these regions were (i) secondary chemical shifts, with agreement between $^{13}C'$, $^{13}C^{\alpha}$, and $^{13}C^{\beta}$ deviations from random coil values, (ii) protection for solvent exchange observed for residues 720–726 and 738–743, suggesting that they are the middle residues in helices, (iii) CD results that are consistent with the presence of helical domains in E2-TM. The structured nature of these segments was echoed in the analysis of relaxation measurements, as they exhibited high squared generalized order parameters and low contributions of local motions. The two helices are connected by a linker segment spanning residues 727–731, including charged residues D728 and R730, and here secondary chemical shifts were similar to random coil values and inconsistent with a helical conformation. However, relaxation rates R_1 and R_2 for this region are not significantly different from those measured for the helical segments, and hetNOE values decrease to ~0.6 but not lower. Overall the linker appears to be only marginally flexible, and significantly more rigid than E2-TM outside the micelle; indeed, the major contribution to relaxation in these residues (as determined by model-free analysis) is the global tumbling of the entire mixed micelle.

Having identified the helix–linker–helix architecture of E2-TM, we continued our study by determining the positioning of E2-TM within the micelle using paramagnetic NMR and cross-relaxation measurements. Spin-labels, molecules carrying an unpaired electron which enhances relaxation in a distance-dependent manner, have been previously employed for high-resolution NMR study of membrane peptides and proteins [48]. In the case of the LPPG/E2-TM mixed micelle the often-used stearate-based nitroxide spin labels [78] were inappropriate, as they resulted in a destabilizing of the micelle, and the small hydrophobic 4-HTB was used instead. Contrary to our initial assumption, 4-HTB exhibited a relatively broad radial distribution in the micelle. Since large effects were observed for several of the terminal E2-TM residues, we concluded that effects exhibited by the linker region (as opposed to the relatively unaffected helical segments) were an indication of the linker's proximity to the micelle perimeter. Titration of the paramagnetic Mn^{2+} ion into the E2-TM sample revealed a pseudocontact shift effect which can only be explained by a binding of the ions to the mixed micelle, most likely to the negatively charged phosphate group. Here, too, the effect was more pronounced for linker residues when compared to the helical segments, confirming the earlier conclusion that the linker lies within the micelle closer to the headgroups rather than at the core of the micelle. Finally, cross-relaxation between the spectrally overlapping methylene protons which span the hydrophobic core of the micelle and E2-TM was strongest for the helical regions but weaker for linker residues, once more establishing their location in the vicinity of the headgroups. Thus, all three measurements were consistent with the conclusion that E2-TM does not traverse the LPPG micelle along its diameter, but rather orients itself in a manner that brings the linker segment in proximity with the micelle headgroup.

Based on the combination of NMR results it is possible to suggest a plausible model for the architecture of the LPPG/E2-TM mixed micelle. We have shown that (i) E2-TM adopts a helix–linker–helix structure, defined by residues 717–726, 727–731, and 732–746, respectively, (ii) the micelle-spanning residues start at W716 and end at the second arginine residues of the C-terminal tail, (iii) the linker residues are unstructured, show a degree of flexibility while remaining ordered relative to the micelle, and (iv) the helix–linker–helix structure is bent, shifting the linker closer to the charged phosphoglycerol headgroups. Fig. 8 schematically summarizes these findings and portrays the ensuing model of the mixed micelle. One possible explanation for the marginal flexibility of the linker may be its length (only 5 residues) and its location between two structured domains. However, another important contribution may be the concomitant requirements of positioning the helical domains in the micelle hydrophobic core while allowing linker residues, specifically their charged sidechains, to extend into the more

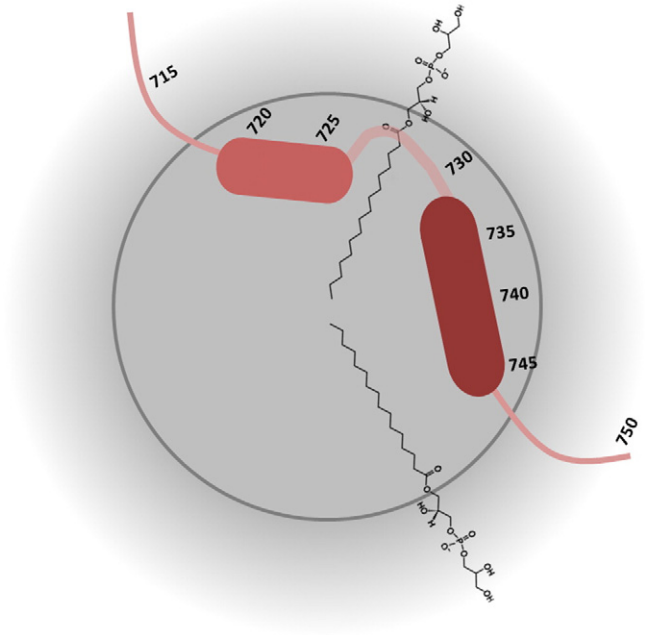

Fig. 8. Summary of NMR-derived global fold and motions of LPPG-embedded E2-TM. The E2-TM peptide (red) is schematically depicted with representative amino acid numbering within an LPPG micelle with hydrophobic core (dark gray) and headgroup region (gradient light gray) shown. An LPPG molecule demonstrates the location of phospholipid nuclei along the micelle radius. Helices and unstructured segments appear in cylinders and lines, respectively, with their thickness proportional to their rigidity.

hydrophilic headgroup region. This could constrain the peptide in a given orientation relative to the micelle, accounting for the model-free interpretation of linker relaxation rates.

The presence of charged residues within the membrane-spanning domain is unusual in MPs, and in most cases indicates a functional role for these residues; in the case of the E1/E2 interaction, residues K370 (of E1) and D728 (of E2) are known to contribute to heterodimerization [26,27]. In drawing conclusions from our results the limitations of this study in LPPG micelles must be recognized. The micelle does not fully reflect the native cell membrane lipid bilayer, and its fluidity may result in deviation from spherical symmetry upon peptide solubilization. However, the size of the LPPG micelle should properly accommodate the E2-TM peptide, suggesting that the helix–linker–helix architecture is a reasonable representation of the E2 glycoprotein TM domain and not an artifact of sample preparation. From our results it is clear that the charged residues exert a significant effect on the structure of the peptide within the micelle, and, presumably, this would be the case in the biological membrane as well. It is plausible to hypothesize that the distorted conformation observed in this study is related to the fold adopted by the HCV E2-TM in the absence of the binding partner E1, or in the case of an E1 mutation abolishing its stabilizing effect (e.g. absence of the K370 residue). This would account for the detrimental effect of such a mutation upon the ability of the E1/E2 heterodimer to efficiently mediate cell fusion. Further studies of the E2-TM peptide, particularly in complex with E1-derived peptides, should be instrumental in shedding additional light on the formation of this key heterodimeric assembly.

5. Conclusions

In this work we have structurally investigated the TM domain of the E2 glycoprotein in a membrane-mimicking environment by a combination of improvements in its expression and NMR methodologies. E2-TM was found to adopt a helix–linker–helix fold, and the charged residues of the linker segment were shown to direct this region to closer proximity with the micelle headgroups. This may reflect the state of the E2 transmembrane domain in the absence of the E1 binding partner or in cases of a mutation at key E1 residues. Currently underway is a more detailed study of the structural description of the E1/E2 interaction in the membrane domain which will greatly enhance our understanding of which structural elements in the heterodimeric complex are critical for its formation.

Funding

This work was supported in part by a research grant to J.H.C. by the Israel Science Foundation (801/09). The 700 MHz spectrometer was purchased with the support of the Converging Technologies Fund. J.H.C. acknowledges support of the Christians for Israel Chair for Medical Research.

Acknowledgments

We wish to thank of Dr. Yoav Peleg (Weizmann Institute of Science, Rehovot, Israel) for his assistance in design and cloning of E2-TM constructs, and Dr. Sharon Ruthstein (Bar Ilan University) for her help with the spin-label experiments. The support of Drs. Hugo Gottlieb and Keren Keinan-Adamsky of the NMR facility is greatly appreciated, and we are thankful to Mr. Israel Tabakman for technical support and maintenance.

Appendix A. Supplementary data

Supplementary data to this article can be found online at http://dx.doi.org/10.1016/j.bbamem.2014.07.023.

References

[1] A. Craxi, G. Laffi, A.L. Zignego, Hepatitis C virus infection: a systemic disease, Mol. Asp. Med. 29 (2008) 85–95.
[2] R. Zampino, A. Marrone, L. Restivo, B. Guerrera, A. Sellitto, L. Rinaldi, C. Romano, L.E. Adinolfi, Chronic HCV infection and inflammation: clinical impact on hepatic and extra-hepatic manifestations, World J. Hepatol. 5 (2013) 528–540.
[3] B. Bartosch, F.-L. Cosset, Cell entry of hepatitis C virus, Virology 348 (2006) 1–12.
[4] T.J. Liang, Current progress in development of hepatitis C virus vaccines, Nat. Med. 19 (2013) 869–878.
[5] J. Halliday, P. Klenerman, E. Barnes, Vaccination for hepatitis C virus: closing in on an evasive target, Expert Rev. Vaccines 10 (2011) 659–672.
[6] E.A. Schaefer, R.T. Chung, Anti-hepatitis C virus drugs in development, Gastroenterology 142 (2012) 1340–1350.e1.
[7] E. De Clercq, The race for interferon-free HCV therapies: a snapshot by the spring of 2012, Rev. Med. Virol. 22 (2012) 392–411.
[8] M.P. Manns, T. von Hahn, Novel therapies for hepatitis C—one pill fits all? Nat. Rev. Drug Discov. 12 (2013) 595–610.
[9] C.W. Kim, K.M. Chang, Hepatitis C virus: virology and life cycle, Clin. Mol. Hepatol. 19 (2013) 17–25.
[10] B.D. Lindenbach, C.M. Rice, The ins and outs of hepatitis C virus entry and assembly, Nat. Rev. Microbiol. 11 (2013) 688–700.
[11] D. Moradpour, F. Penin, Hepatitis C virus proteins: from structure to function, Curr. Top. Microbiol. Immunol. 369 (2013) 113–142.
[12] A. Op De Beeck, C. Voisset, B. Bartosch, Y. Ciczora, L. Cocquerrel, Z. Keck, S. Foung, F.-L. Cosset, J. Dubuisson, Characterization of functional hepatitis C virus envelope glycoproteins, J. Virol. 78 (2004) 2994–3002.
[13] L. Kong, E. Giang, T. Nieusma, R.U. Kadam, K.E. Cogburn, Y. Hua, X. Dai, R.L. Stanfield, D.R. Burton, A.B. Ward, I.A. Wilson, M. Law, Hepatitis C virus E2 envelope glycoprotein core structure, Science 342 (2013) 1090–1094.
[14] A. Wahid, F. Helle, V. Descamps, G. Duverlie, F. Penin, J. Dubuisson, Disulfide bonds in hepatitis C virus glycoprotein E1 control the assembly and entry functions of E2 glycoprotein, J. Virol. 87 (2013) 1605–1617.
[15] S. Rajesh, P. Sridhar, B.A. Tews, L. Fénéant, L. Cocquerel, D.G. Ward, F. Berditchevski, M. Overduin, Structural basis of ligand interactions of the large extracellular domain of tetraspanin CD81, J. Virol. 86 (2012) 9606–9616.
[16] J. Fraser, I. Boo, P. Poumbourios, H.E. Drummer, Hepatitis C virus (HCV) envelope glycoproteins E1 and E2 contain reduced cysteine residues essential for virus entry, J. Biol. Chem. 286 (2012) 31984–31992.
[17] F. Douam, V.L. Thi, G. Maurin, J. Fresquet, D. Mompelat, M.B. Zeisel, T.F. Baumert, F.L. Cosset, D. Lavillette, A critical interaction between E1 and E2 glycoproteins determines binding and fusion properties of hepatitis C virus during cell entry, Hepatology 59 (3) (2014) 768–778.

[18] E. Falkowska, F. Kajumo, E. Garcia, J. Reinus, T. Dragic, Hepatitis C virus envelope glycoprotein E2 glycans modulate entry, CD81 binding, and neutralization, J. Virol. 81 (2007) 8072–8079.
[19] M.J. Farquhar, H.J. Harris, J.A. McKeating, Hepatitis C virus entry and the tetraspanin CD81, Biochem. Soc. Trans. 39 (2011) 532–536.
[20] G.A. Sautto, R.A. Diotti, M. Clementi, New therapeutic options for HCV infection in the monoclonal antibody era, New Microbiol. 35 (2012) 387–397.
[21] R. Liu, M. Tewari, R. Kong, R. Zhang, P. Ingravallo, R. Ralston, A peptide derived from hepatitis C virus E2 envelope protein inhibits a post-binding step in HCV entry, Antiviral Res. 86 (2010) 172–179.
[22] Z.L. Qin, H.P. Ju, W.B. Wang, H. Ren, M. Guan, P. Zhao, Z.T. Qi, The Arg719 residue at the C-terminal end of the stem region in hepatitis C virus JFH-1 E2 glycoprotein promotes viral infection, Virus Res. 172 (2010) 1–8.
[23] C. Montpellier, B.A. Tews, J. Poitrimole, V. Rocha-Perugini, V. D'Arienzo, J. Potel, X.A. Zhang, E. Rubinstein, J. Dubuisson, L. Cocquerel, Interacting regions of CD81 and two of its partners, EWI-2 and EWI-2wint, and their effect on hepatitis C virus infection, J. Biol. Chem. 286 (2011) 13954–13965.
[24] A. Albecka, R. Montserret, T. Krey, A.W. Tarr, E. Diesis, J. Ball, V. Descamps, G. Duverlie, F. Rey, F. Penin, J. Dubuisson, Identification of new functional regions in hepatitis C virus envelope glycoprotein E2, J. Virol. 85 (2011) 1777–1792.
[25] L. Cocquerel, C. Wychowski, F. Minner, F. Penin, J. Dubuisson, Charged residues in the transmembrane domains of hepatitis C virus glycoproteins play a major role in the processing, subcellular localization, and assembly of these envelope proteins, J. Virol. 74 (2000) 3623–3633.
[26] Y. Ciczora, N. Callens, C. Montpellier, B. Bartosch, F.-L. Cosset, A. Op De Beeck, J. Dubuisson, Contribution of the charged residues of hepatitis C virus glycoprotein E2 transmembrane domain to the functions of the E1 E2 heterodimer, J. Gen. Virol. 86 (2005) 2793–2798.
[27] Y. Ciczora, N. Callens, F. Penin, E.-I. Pecheur, J. Dubuisson, Transmembrane domains of hepatitis C virus envelope glycoproteins: residues involved in the E1E2 Heterodimerization and involvement of these domains in virus entry, J. Virol. 81 (2007) 2372–2381.
[28] L. Fagerberg, K. Jonasson, G. von Heijne, M. Uhlen, L. Berglund, Prediction of the human membrane proteome, Proteomics 10 (2010) 1141–1149.
[29] N. Bordag, S. Keller, Alpha-helical transmembrane peptides: a "divide and conquer" approach to membrane proteins, Chem. Phys. Lipids 163 (2010) 1–26.
[30] P. Hubert, P. Sawma, J.P. Duneau, J. Khao, J. Henin, D. Bagnard, J. Sturgis, Single-spanning transmembrane domains in cell growth and cell–cell interactions: more than meets the eye? Cell Adhes. Migr. 4 (2) (2010) 313–324.
[31] I. Ubarretxena-Belandia, D.M. Engelman, Helical membrane proteins: diversity of functions in the context of simple architecture, Curr. Opin. Struct. Biol. 11 (2001) 370–376.
[32] E.V. Bocharov, P.E. Volynsky, K.V. Pavlov, R.G. Efremov, A.S. Arseniev, Structure elucidation of dimeric transmembrane domains of bitopic proteins, Cell Adh. Migr. 4 (2) (2010) 284–298.
[33] R.D. Krueger-Koplin, P.L. Sorgen, S.T. Krueger-Koplin, I.O. Rivera-Torres, S.M. Cahill, D.B. Hicks, L. Grinius, T.A. Krulwich, M.E. Girvin, An evaluation of detergents for NMR structural studies of membrane proteins, J. Biomol. NMR 28 (2004) 43–57.
[34] R.C. Page, J.D. Moore, H.B. Nguyen, M. Sharma, R. Chase, F.P. Gao, C.K. Mobley, C.R. Sanders, L. Ma, F.D. Sonnichsen, S. Lee, S.C. Howell, S.J. Opella, T.A. Cross, Comprehensive evaluation of solution nuclear magnetic resonance spectroscopy sample preparation for helical integral membrane proteins, J. Struct. Funct. Genom. 7 (2006) 51–64.
[35] S.F. Poget, M.E. Girvin, Solution NMR of membrane proteins in bilayer mimics: small is beautiful, but sometimes bigger is better, Biochim. Biophys. Acta 1768 (2007) 3098–3106.
[36] D. Warschawski, A.A. Arnold, M. Beaugrand, A. Gravel, E. Chartrand, I. Marcotte, Choosing membrane mimetics for NMR structural studies of transmembrane proteins, Biochim. Biophys. Acta 1808 (2009) 1957–1974.
[37] F. Hagn, M. Etzkorn, T. Raschle, G. Wagner, Optimized phospholipid bilayer nanodiscs facilitate high-resolution structure determination of membrane proteins, J. Am. Chem. Soc. 135 (2013) 1919–1925.
[38] Z.O. Shenkarev, E.N. Lyukmanova, I.O. Butenko, L.E. Petrovskaya, A.S. Paramonov, M.A. Shulepko, O.V. Nekrasova, M.P. Kirpichnikov, A.S. Arseniev, Lipid-protein nanodiscs promote in vitro folding of transmembrane domains of multi-helical and multimeric membrane proteins, Biochim. Biophys. Acta 1828 (2013) 776–784.
[39] Y. Su, S. Li, M. Hong, Cationic membrane peptides: atomic-level insight of structure–activity relationships from solid-state NMR, Amino Acids 44 (2013) 821–833.
[40] A. Ramamoorthy, Beyond NMR spectra of antimicrobial peptides: dynamical images at atomic resolution and functional insights, Solid State Nucl. Magn. Reson. 35 (2009) 201–207.
[41] E. Strandberg, P. Tremouilhac, P. Wadhwani, A.S. Ulrich, Synergistic transmembrane insertion of the heterodimeric PGLa/magainin 2 complex studied by solid-state NMR, Biochim. Biophys. Acta 1788 (2009) 1667–1679.
[42] B. Bechinger, J.M. Resende, C. Aisenbrey, The structural and topological analysis of membrane-associated polypeptides by oriented solid-state NMR spectroscopy: established concepts and novel developments, Biophys. Chem. 153 (2011) 115–125.
[43] A.G. Palmer III, C.D. Kroenke, J.P. Loria, Nuclear magnetic resonance methods for quantifying microsecond-to-millisecond motions in biological macromolecules, Methods Enzymol. 339 (2001) 204–238.
[44] F. Ferrage, Protein dynamics by ^{15}N nuclear magnetic relaxation, Methods Mol. Biol. 831 (2012) 141–163.
[45] G.M. Clore, C. Tang, J. Iwahara, Elucidating transient molecular interactions using paramagnetic relaxation enhancement, Curr. Opin. Struct. Biol. 17 (2007) 603–616.
[46] K.J. Walters, A.E. Ferentz, B.J. Hare, P. Hidalgo, A. Jasanoff, H. Matsuo, G. Wagner, Characterizing protein-protein complexes and oligomers by nuclear magnetic resonance spectroscopy, Methods Enzymol. 339 (2001) 238–258.
[47] H. Takahashi, T. Nakanishi, K. Kami, Y. Arata, I. Shimada, A novel NMR method for determining the interfaces of large protein–protein complexes, Nat. Struct. Biol. 7 (2000) 220–223.
[48] E. Schrank, G.E. Wagner, K. Zangger, Solution NMR studies on the orientation of membrane-bound peptides and proteins by paramagnetic probes, Molecules 18 (2013) 7407–7435.
[49] T. Qureshi, N.K. Goto, Contemporary methods in structure determination of membrane proteins by solution NMR, Top. Curr. Chem. 326 (2012) 123–185.
[50] H. Zazrin, H. Shaked, J.H. Chill, Architecture of the hepatitis C virus E1 glycoprotein transmembrane domain studied by NMR, Biochim. Biophys. Acta 1838 (2013) 784–792.
[51] M. Cai, Y. Huang, K. Sakaguchi, G.M. Clore, A.M. Gronenborn, R. Craigie, An efficient and cost-effective isotope labeling protocol for proteins expressed in *Escherichia coli*, J. Biomol. NMR 11 (1998) 97–102.
[52] Y. Peleg, T. Unger, Application of high-throughput methodologies to the expression of recombinant proteins in *E. coli*, Methods Mol. Biol. 426 (2008) 197–208.
[53] T. Unger, Y. Jacobovitch, A. Dantes, R. Bernheim, Y. Peleg, Applications of the Restriction Free (RF) cloning procedure for molecular manipulations and protein expression, J. Struct. Biol. 172 (2010) 34–44.
[54] L. Whitmore, B.A. Wallace, Protein secondary structure analyses from circular dichroism spectroscopy: methods and reference databases, Biopolymers 89 (2004) 392–400.
[55] M. Salzmann, G. Wider, K. Pervushin, H. Senn, K. Wuthrich, TROSY-type triple-resonance experiments for sequential NMR assignments of large proteins, J. Am. Chem. Soc. 121 (1999) 844–848.
[56] J.B. Hall, D. Fushman, Characterization of the overall and local dynamics of a protein with intermediate rotational anisotropy: differentiating between conformational exchange and anisotropic diffusion in the B3 domain of protein G, J. Biomol. NMR 27 (2003) 261–275.
[57] J.B. Hall, D. Fushman, Variability of the ^{15}N chemical shielding tensors in the B3 domain of protein G from ^{15}N relaxation measurements at several fields. Implications for backbone order parameters, J. Am. Chem. Soc. 128 (2006) 7855–7870.
[58] A.J. Perez-Berna, M.R. Moreno, J. Guillen, A. Bernabeu, J. Villalain, The membrane-active regions of the hepatitis C virus E1 and E2 envelope glycoproteins, Biochemistry 45 (2006) 3755–3768.
[59] A.J. Pérez-Berná, J. Guillén, M.R. Moreno, A.I. Gómez-Sánchez, G. Pabst, P. Laggner, J. Villalaín, Interaction of the most membranotropic region of the HCV E2 envelope glycoprotein with membranes: biophysical characterization, Biophys. J. 94 (2008) 4737–4750.
[60] C.R. Sanders, F.D. Sonnichsen, Solution NMR of membrane proteins: practice and challenges, Magn. Reson. Chem. 44 (2006) S24–S40.
[61] A. Bax, S. Grzesiek, Methodological advances in protein NMR, Acc. Chem. Res. 26 (1993) 131–138.
[62] M. Berjanskii, P. Tang, J. Liang, J.A. Cruz, J. Zhou, Y. Zhou, E. Bassett, C. MacDonell, P. Lu, G. Lin, D.S. Wishart, GeNMR: a web server for rapid NMR-based protein structure determination, Nucleic Acids Res. 37 (2009) W670–W677.
[63] A. Cavalli, X. Salvatella, C.M. Dobson, M. Vendruscolo, Protein structure determination from NMR chemical shifts, Proc. Natl. Acad. Sci. U. S. A. 104 (2007) 9615–9620.
[64] S. Raman, O.F. Lange, P. Rossi, M. Tyka, X. Wang, J. Aramini, G. Liu, T.A. Ramelot, A. Eletsky, T. Szyperski, M.A. Kennedy, J. Prestegard, G.T. Montelione, D. Baker, NMR structure determination for larger proteins using backbone-only data, Science 327 (2010) 1014–1018.
[65] Y. Shen, O. Lange, F. Delaglio, P. Rossi, J.M. Aramini, G. Liu, A. Eletsky, Y. Wu, K.K. Singarapu, A. Lemak, A. Ignatchenko, C.H. Arrowsmith, T. Szyperski, G.T. Montelione, D. Baker, A. Bax, Consistent blind protein structure generation from NMR chemical shift data, Proc. Natl. Acad. Sci. U. S. A. 105 (2008) 4685–4690.
[66] Y. Shen, F. Delaglio, G. Cornilescu, A. Bax, TALOS+: a hybrid method for predicting protein backbone torsion angles from NMR chemical shifts, J. Biomol. NMR 44 (2009) 213–223.
[67] N.A. Farrow, O. Zhang, A. Szabo, D.A. Torchia, L.E. Kay, Spectral density function mapping using ^{15}N relaxation data exclusively, J. Biomol. NMR 6 (1995) 153–162.
[68] J.W. Peng, G. Wagner, Mapping of the spectral densities of N–H bond motions in eglin-C using heteronuclear relaxation measurements, Biochemistry 31 (1992) 8571–8586.
[69] A.V. Buevich, U.P. Shinde, M. Inouye, J. Baum, Backbone dynamics of the natively unfolded pro-peptide of subtilisin by heteronuclear NMR relaxation studies, J. Biomol. NMR 20 (2001) 233–249.
[70] G. Lipari, A. Szabo, Model-free approach to the interpretation of nuclear magnetic resonance relaxation in macromolecules. 1. Theory and range of validity. 2. Analysis of experimental results, J. Am. Chem. Soc. 104 (1982) 4546–4570.
[71] A.M. Mandel, M. Akke, A.G. Palmer III, Backbone dynamics of *Escherichia coli* ribonuclease HI: correlations with structure and function in an active enzyme, J. Mol. Biol. 246 (1995) 144–163.
[72] J.J. Chou, J.L. Baber, A. Bax, Characterization of phospholipid mixed micelles by translational diffusion, J. Biomol. NMR 29 (2003) 299–308.
[73] C. Fernandez, C. Hilty, G. Wider, K. Wuthrich, Lipid–protein interactions in DHPC micelles containing the integral membrane protein OmpX investigated by NMR spectroscopy, Proc. Natl. Acad. Sci. U. S. A. 99 (2002) 13533–13537.

[74] T.S. Ulmer, A. Bax, Comparison of structure and dynamics of micelle-bound human a-synuclein and Parkinson disease variant, J. Biol. Chem. 280 (2005) 43179–43187.
[75] J.H. Chill, J.M. Louis, C. Miller, A. Bax, NMR study of the tetrameric KcsA potassium channel in detergent micelles, Prot. Sci. 15 (2006) 684–698.
[76] M. Itaya, I.C. Brett, S.O. Smith, Synthesis, purification, and characterization of single helix membrane peptides and proteins for NMR spectroscopy, Methods Mol. Biol. 831 (2012) 333–357.
[77] K. Yamamoto, M. Gildenberg, S. Ahuja, S.-C. Im, P. Pearcy, L. Waskell, A. Ramamoorthy, Probing the transmembrane structure and topology of microsomal cytochrome-p450 by solid-state NMR on temperature-resistant bicelles, Sci. Rep. 3 (2013) 2556.
[78] C. Hilty, G. Wider, C. Fernández, K. Wuthrich, Membrane protein-lipid interactions in mixed micelles studied by NMR spectroscopy with the use of paramagnetic reagents, ChemBioChem 5 (2004) 467–473.